FAST DIFFUSION ALONG DEFECTS AND CORRUGATIONS IN PHOSPHOLIPID $P_{\beta'}$ LIQUID CRYSTALS

MARILYN B. SCHNEIDER, WINSTON K. CHAN, AND WATT W. WEBB
Department of Physics and Department of Applied and Engineering Physics, Cornell University, Ithaca, New York 14853

ABSTRACT The diffusion of a fluorescent lipid analogue in liquid crystals of the anisotropic $P_{\beta'}$ phase of dimyristoylphosphatidylcholine (DMPC) had been found to be highly variable, suggesting structural defect pathways. Fluorescence photobleaching recovery (FPR) experiments imply two effective diffusion pathways with coefficients differing by at least 100. This is consistent with fast diffusion along submicroscopic bands of disordered material ("defects") in the bilayer corrugations characteristic of this phase. Due to strains during transformation from the L_α phase, the axis of the corrugations is ordinarily disrupted by mosaic patches rotationally disoriented within the mean plane of the molecular bilayers, although larger oriented domains are sometimes adventitiously aligned into microscopically visible striped textures. The corrugations are also systematically aligned along positive disclinations pairs or "oily streaks." Thus, fast diffusion occurs parallel to the disclination lines and along the textured stripes. FPR results yield an upper limit on the effective diffusion coefficient in the ordered material of $D \leq 2 \times 10^{-16}$ cm^2/s at 22°C, $D \leq 3 \times 10^{-17}$ cm^2/s at 13°C. In contrast the diffusion coefficient along defect pathways where disordered ribbons are aligned is $D \sim 4 \times 10^{-11}$ cm^2/s at 16°C.

INTRODUCTION

Phospholipids, a major component of cell membranes, can form smectic lyotropic liquid crystals consisting of symmetric lipid bilayers intercalated with water. Above the gel or main phase transition temperature the liquid crystals of phosphatidylcholine form an L_α phase, a smectic A structure where the intermolecular order in each half of a bilayer is limited to the short range order of a two-dimensional liquid, and the intramolecular *trans*-gauche rotational order of the hydrocarbon chains is low. As the temperature is lowered at full hydration, some phospholipids, particularly dimyristoylphosphatidylcholine (DMPC) and dipalmitoylphosphatidylcholine (DPPC), undergo a first-order phase transition (1, 2) to the $P_{\beta'}$ phase. In this phase, it is usually supposed that the hydrocarbon chains are frozen into a nearly all *trans* configuration (3–5): the molecules are packed in a two-dimensional hexagonal lattice (2, 6, 7), the intralayer self-diffusion coefficient is small (8–11), and the molecular axis is believed to be tilted with respect to the local normal to the bilayer (2, 6, 7), but there is some controversy about the tilt (12, 13). The $P_{\beta'}$ phase is characterized by the presence of intralayer corrugations. X-ray diffraction experiments find the periodicity to be 140 Å (2, 6, 7, 13–15). Freeze fracture replicas scanned with an electron microscope often have regions with periodicities of ~130 Å or 250 Å (16–22). The structural details of the corrugations are undetermined: some models predict a sinusoidal modulation (2, 6, 7, 13, 23); others predict a sawtooth modulation (19–21, 24, 25). The corrugation amplitude is still disputed: The minimum reported amplitude is ~8 Å (7) and the maximum reported amplitude is 25 Å (13). At a slightly lower temperature there is a second phase transition, the pretransition, which consists of a crystallographic change to the $L_{\beta'}$ phase. This phase is similar to a smectic *G*. Recently (26–28), a fourth phase has been discovered at a lower temperature. In addition to the biophysical significance of the lipid system (4, 29), these phases have current physical interest due to their two-dimensional intermolecular order (30–32).

Molecular self-diffusion studies can yield valuable information about intralayer molecular ordering (4, 8–11, 29). The manner in which the poorly understood corrugations of the biomolecular layers in the $P_{\beta'}$ phase affect diffusion measurements motivated this work. The lateral self-diffusion coefficient, *D*, has been measured in many of the L_α phases using fluorescence photobleaching recovery (FPR) (8, 9) and magnetic resonance spectroscopy (33–35) and has been found to be $\sim 5 \times 10^{-8}$ cm^2/s. As expected, there is a dramatic decrease in *D* as the phospholipid is cooled into the $P_{\beta'}$ phase (9); *D* has been reported to vary up to $\sim 1 \times 10^{-10}$ cm^2/s, just below the transition temperature (10, 11). However, the FPR studies on large planar preparations of the $P_{\beta'}$ phase reported here indicate a more complicated situation; we find two very different coexisting diffusivities. We propose that inhomogeneous intermolecular disorder associated with the ridges

Dr. Chan's present address is Bell Labs, Murray Hill, NJ 07974.

and furrows of the bilayer corrugations in the $P_{\beta'}$ phase is responsible for the variability of reported values of D and that the true diffusion coefficient in a well aligned $P_{\beta'}$ crystal would be highly anisotropic within the plane of the bilayer. This problem limits the value of multilayer specimens as models for diffusion in the low temperature phases of DMPC membranes but reveals an interesting physical effect that may have potential membrane analogues.

We hypothesize that the diffusive process detected in an FPR experiment in the corrugated $P_{\beta'}$ phase is that of a tracer molecule diffusing into a material whose structure consists of parallel bands of fast and slow diffusivities. The appropriate analysis depends on the widths and relative diffusivities of the bands and on the distribution of band orientations within the specimens and on the time scale of an observation. Detailed analysis of diffusion in inhomogeneous defect structures (36–40) shows that a measurement falls into one of three categories depending on these characteristics (36): Type A diffusion is characterized by a single, volume-weighted average diffusion coefficient (37). It describes the system if the slow and fast diffusion coefficients are approximately equal or if the experimental time is long enough for a diffusing particle to have entered, migrated in, and departed a number of fast bands. Type B diffusion, the intermediate and most complicated case, describes the system if the characteristic diffusion length in the slow band during the time of observation is comparable to the characteristic dimensions of a fragment of the slow band, that is, the separation between fast bands. This case has been analyzed in detail (38–40). Type C diffusion, characterized by diffusion principally along the fast bands, describes the system at short times or in the case when diffusion in the fast band is very much faster than diffusion in the slow band. The diffusion measurements reported here can be accounted for by Type C diffusion. Owicki and McConnell (41) have analyzed the effective diffusion rates in a banded structure. Their analysis is for Type A diffusion and is not applicable to our measurements nor to other membrane or liquid crystal experiments on pure phospholipids of which we are aware.

We have devised a simple means to observe inhomogeneous anisotropic diffusion behavior. Ordinarily the unit cell shape change at the phase transformation between the L_α and $P_{\beta'}$ phase causes strains in macroscopic specimens that fragment the $P_{\beta'}$ phase into a mosaic with variable orientations of the domains, which complicates the analysis of diffusion in the fast bands. If the corrugations are aligned over distances of tens of micrometers, the diffusion in the fast bands can be directly observed. Photographs of the pattern of diffusive motion of fluorophore from the perimeter of large areas following photobleaching show this fast diffusion along visible wide paired disclinations (oily streaks) (42, 43, and Schneider and Webb, manuscript in preparation) traversing the bleached zone. Measurements of the time course of fluorescence recovery provided data for analysis with a simple one-dimensional diffusion model. Optical microscopy reveals localized areas of a texture of the $P_{\beta'}$ phase showing macroscopically visible parallel stripes.

EXPERIMENTAL METHODS

Methods of Specimen Preparation

Multilamellar, homeotropically aligned (molecular layers generally parallel to the glass slides) liquid crystal specimens of the L_α phase are formed from a stock solution of 25 mg DMPC (Applied Science Div., Milton Roy Co., State College, PA) and 1×10^{-5} to 5×10^{-4} mole fraction 3,3'-dioctadecylindocarbocyanine iodide (diI) (44), a fluorescent lipid analogue (generous gift of Dr. Alan S. Waggoner) in 3 ml of 2:1 vol/vol chloroform/methanol solution. Two methods are used in the formation of the specimens. In the first method, a lipid deposit is formed by spreading a droplet of stock solution containing 400 μg of lipid in the 100 μm deep well of a polished quartz slide. The deposit is dried at 37°C for at least 2 h, and then hydrated either with 30 μl of phosphate-buffered saline solution without calcium and magnesium or with doubly distilled water. A cover glass is carefully placed over the well and sealed with a mixture of Apezion M grease (James G. Biddle Co., Plymouth Meeting, PA) and paraffin wax. This leaves the top surface of the liquid crystal deposit in contact with excess water and otherwise unconstrained. The specimen remains in the oven without disturbance for at least 15 min after hydration. In the second method, the specimen is formed similarly on a flat microscope slide and the cover glass is placed directly on the liquid crystal specimen. A 7 g weight is placed on top, and the specimen is left in a water-saturated atmosphere for several days at 30°C before sealing with wax. Both the cover glass and slide are cleaned in hot chromic-sulfuric acid just before use. Our diffusion results do not differ significantly with (small) variations in dye concentrations, hydrating solutions, or preparation methods.

Specimen Characterization

In the L_α phase, both fluorescence and phase-contrast microscopy show smooth multilamellar regions 50–100 μm across and 100–1,000 bilayers (0.5 to 5 μm) thick. Thicknesses are determined by comparison of the fluorescence intensity with that of a black lipid measure (9) or the change of fluorescence intensity across elementary edge dislocations (45, 46). These determinations agree with thicknesses calculated from the amount of lipid deposited. The thinner specimens are those with excess water above them because most of the lipid has formed liposomes (multilayer vesicles) in the excess water, possibly to minimize elastic splay energy (47), and the liposomes have floated away. The smooth regions divide into micrometer-sized domains when the specimen is cooled below the main transition temperature at 23°C. The FPR experiments below the phase transition are performed in regions that appear smooth under fluorescence over 3–4 μm.

FPR Diffusion Measurements

The FPR method is commonly used in biophysics to measure the lateral diffusion coefficient of a fluorescent tracer (8, 9, 11,48–50). The beam of a laser operating in the TEM_{00} mode is focused onto a small spot in the sample (51). The laser intensity is momentarily increased by several orders of magnitude to photobleach some of the dye molecules in the illuminated spot. The fluorescence gradually recovers as fresh fluorophore diffuses into the photobleached area. For isotropic and homogeneous diffusion in two dimensions, the fluorescence intensity normalized by the pre-bleach fluorescence intensity, t s after photobleaching, is (49)

$$F_2(t,\tau_{D2}) = \sum_{n=0}^{\infty}[(-K)^n/n!]\,[1 + n(1 + 2t/\tau_{D2})]^{-1} \quad (1)$$

where e^{-K}/K is the fraction of the original fluorophore remaining unbleached at $t = 0$ and τ_{D2} is the characteristic recovery time. D_2, the lateral self-diffusion coefficient of the fluorophore is related to τ_{D2} and w_0, the laser beam radius, by $D_2 = w_0^2/4\tau_{D2}$. In some cases, it is useful to define a phenomenological parameter f that describes the fraction of the intensity that recovers according to Eq. 1. Thus f is associated with the fraction of dye that diffuses in the timescale of the experiment and $1-f$ with the fraction that does not diffuse in this timescale.

Restriction of diffusion to one direction (with the same circular symmetry of illumination) quantitatively changes the time course of fluorescence photobleaching recovery. The corresponding one-dimensional solution of the recovery problem for the same conditions specified above yields

$$F_1(t,\tau_{D1}) = \sum_{n=0}^{\infty}[(-K)^n/n!]\,[1 + n(1 + 2t/\tau_{D1})]^{(-1/2)} \quad (2)$$

where the fraction of original fluorophore remaining unbleached at $t = 0$ is now $\Sigma[(-K)^n/n!]\,(1+n)^{(-1/2)}$. The one-dimensional diffusion coefficient of the fluorophore is still related to the characteristic recovery time by $D_1 = w_0^2/4\tau_{D1}$. This one-dimensional solution is appropriate, for example, to model fast diffusion along a parallel array of isolated line defects if bulk diffusion is negligible during the time course of the experiment.

Measurements of Diffusion in Representative Multilayers Using FPR

When the specimen is in the L_α phase, the experimental curves generally fit Eq. 1 with $f = 1$ and $D_2 = 5 \times 10^{-8}$ cm^2/s, consistent with complete, isotropic diffusibility in the plane of the bilayers. In contrast, when the specimen is in the $P_{\beta'}$ phase, the experimental curves show incomplete recovery on the timescale of the experiments and do not usually fit Eq. 1 or 2 even with $f < 1$.

In an attempt to improve the fit, a weighted sum of two recovery curves is invoked as a model for two parallel, independent diffusion processes. Thus

$$F(t) = f\,F(t,\tau_f) + (1 - f)\,F(t,\tau_s). \quad (3)$$

The quality of the fit is insensitive to the choice of the diffusion dimensionality in the functional form for F. Either the two-dimensional (Eq. 1) or one-dimensional (Eq. 2) expressions may be used in Eq. 3 with four fitting parameters, D_f, D_s, K, and f. For example, Fig. 1 shows a typical recovery curve fitted to Eq. 3, assuming both diffusion processes

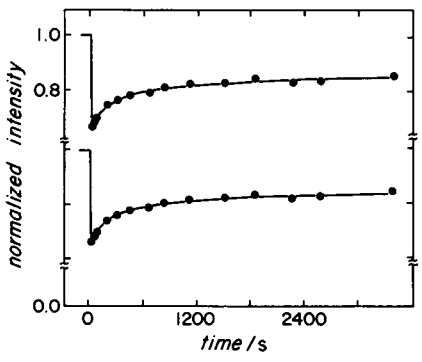

FIGURE 1 Typical FPR recovery data (•) for diI in DMPC multilayers in the $P_{\beta'}$ phase showing apparent incomplete recovery. Curves are fitted to Eq. 3 using the two-dimensional functional form for F (Eq. 1) yielding $D_f = 1.2 \times 10^{-11}$ cm^2/s, $f = 0.51$ and (*inset*) the one-dimensional functional form for F (Eq. 2) yielding $D_f = 1.9 \times 10^{-11}$ cm^2/s, $f = 0.65$. Measured at 16.1°C. Fluorescence intensity in relative units; the zero is shown for the top curve. Laser beam radius was 0.95 μm.

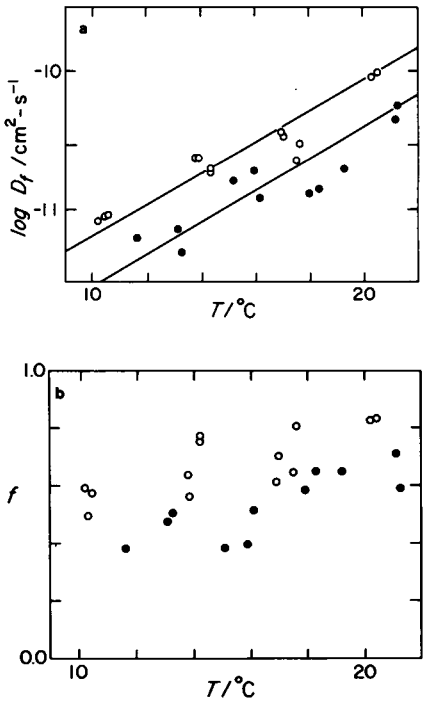

FIGURE 2 Results of FPR measurements on two DMPC multilayer specimens in the $P_{\beta'}$ phase analyzed using the two-dimensional diffusion functional form for F (Eq. 1) in Eq. 3 to obtain D_f and f. ●, specimen one; ○, specimen two. (*a*) log(D_f) vs. T. (*b*) f vs. T.

are two dimensional (Eq. 1). The inset shows the fit if both processes are assumed to be one dimensional (Eq. 2). Both fits match the data equally well. The FPR data cannot be used to determine the dimensionality of the diffusive path, but can give a good quantitative measure of the characteristic times.

In Fig. 2 *a*, the two-dimensional fitted values of D_f are plotted as log(D_f) vs. T for two specimens; corresponding values of f are plotted vs. T in Fig. 2 *b*. Generally, the values of D_f for various specimens fall within a factor of 3 and always follow the same temperature dependence. If Eq. 2 is used to fit the data the magnitude of D_f appears to double, but retains the same temperature dependence and magnitude of f as in the two-dimensional fits. If w_0 is increased to $4w_0$ by changing microscope objectives (51), τ_f increases by a factor of 16, verifying D_f is proportional to $w_0^2/4\tau_f$. The average value of D_f from all of the fits to Eq. 1 at one temperature is

$$D_f = 4 \pm 3 \times 10^{-11}\ \text{cm}^2/\text{s at } 16°\text{C}. \quad (4)$$

Only an estimate for D_s is possible because the 1-h time of an experiment is generally less than a characteristic time of the slow component of the recovery (Type C diffusion [36]). Experimental drifts that spuriously appear to speed recovery prevented longer observations. At 22°C, just below the main transition temperature, $D_s \leq 4 \times 10^{-12}$ cm^2/s; at 13°C, $D_s \leq 5 \times 10^{-13}$ cm^2/s. Lower limits on D_s are deduced in A Banded Disorder Model of the $P_{\beta'}$ Phase section. The relative amount of each component varies erratically but is ~50%.

Diffusion Along Microscopic Defects

It is well known that line defects in many solids are fast diffusion channels and Asher and Pershan (43) have suggested that oily streaks are fast diffusion channels in liquid crystals. We observe this effect in the oily streak or paired disclinations (shown schematically in Fig. 3) (42, 43, and Schneider and Webb, manuscript in preparation), the typical linear defect found in multilayer samples. As an example, the photomicrographs

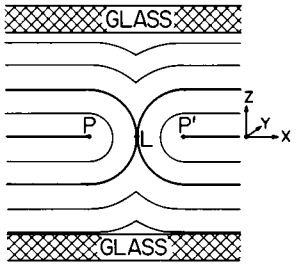

FIGURE 3 Schematic of molecular planes around paired disclinations or oily streak structure in a smectic phase. The white areas are the bilayers. Axes marked for notation in $P_{\beta'}$ phase. The two positive disclination lines, P and P', run parallel to the y axis in our notation for these defects in this phase.

in Fig. 4 *b–d*, show the pattern of fluorescence recovery after a 70-μm diam spot, traversed by two paired disclinations, has been photobleached by a 30-min exposure to a 100-W high-pressure mercury lamp. A phase-contrast photomicrograph showing the location of the paired disclinations is shown in Fig. 4 *a*. The experiment was performed at 18°C after the specimen had been held at this temperature in the presence of excess water for 1 d. The fast recovery of fluorescence intensity that occurs along the paired disclination indicates fast diffusion along these defects.

The fast diffusion pathways along large paired disclinations are wide enough that the fluorescence recovery inside the defect itself can be monitored. In analyzing it, the effect of the surrounding matrix area can be neglected if diffusion there is sufficiently slow. In this limit the case becomes a one-dimensional problem with an initial concentration in the unbleached area ($z < 0$) of $C = C_0$ and an initial concentration in the bleached area ($z > 0$) of $C = 0$. The diffusion process is turned on at $t = 0$. (In most of the experiments, half the illuminated field [$z > 0$] is photobleached; the paired disclinations run perpendicular to the interface [at $z = 0$].) The solution is (52)

$$C(z,t) = (C_0/2)erfc\,\{z/[2(D_{pd}\,t)^{1/2}]\} \qquad (5)$$

where *erfc* x is the complementary error function of argument x and D_{pd} is the diffusion coefficient along the line defect. The distance, $z(C)$, that a given concentration contour advances along the z axis is proportional to $t^{1/2}$.

In Fig. 5, $z(C)$ is plotted as a function of $t^{1/2}$ for two typical paired disclinations at 16°C. $z(C)$ is measured by projecting the negatives of the fluorescence photomicrographs onto a tracing made from the phase contrast picture photographed at the same time. After the two frames are accurately aligned, the distance $z(C)$ along the defect is estimated from the density of the film grains. The linear fit to the data points (Fig. 5) is consistent with this simple diffusion model. The scatter of the data precludes stringent tests of the model such as the approximation that D_{pd} is constant across the width of the defect.

The value of the defect diffusion coefficient D_{pd} determined in the above manner from 10 paired disclinations at 16°C is

$$D_{pd} = 3 \pm 2 \times 10^{-11}\ \mathrm{cm^2/s}. \qquad (6)$$

From the observation that the bleaching boundary becomes noticeably diffuse after 6 h of recovery, and the assumption that this diffusion is due to homogeneous diffusion, an estimate can be obtained for the effective diffusion coefficient in the surrounding matrix of $D_m \sim L^2/4t \sim 10^{-13}$ cm^2/s where $L \sim 2\ \mu$m is half the width of the diffuse interface and t is 6 h. A different interpretation of this diffuseness is given in the next section; it suggests that this value of D is an upper limit for bulk diffusion in a random mosaic.

Sometimes rapid recovery is observed in regions where no paired disclinations nor other large defects are visible. This is explained in the following section. Liquid crystal flow during recovery is sometimes detected but can be recognized and separated from the diffusion processes.

Observations of Fast Diffusion in Regions of Aligned Texture

The texture of a crystallographic in-plane orientation of the corrugation direction in the $P_{\beta'}$ phase is revealed in the thicker specimens using three methods: (*a*) the specimen's birefringence when observed between crossed polarizers (Fig. 6, *a* and *b*); (*b*) phase contrast microscopy (Fig. 6, *c* and *d*); and (*c*) preferential fluorophore absorption of polarized exciting light observed by fluorescence microscopy (Fig. 6, *e* and *f*). We believe the visible texture is due to preferential alignment of the 140 Å corrugations over areas large enough to be resolved in the light microscope. The texture

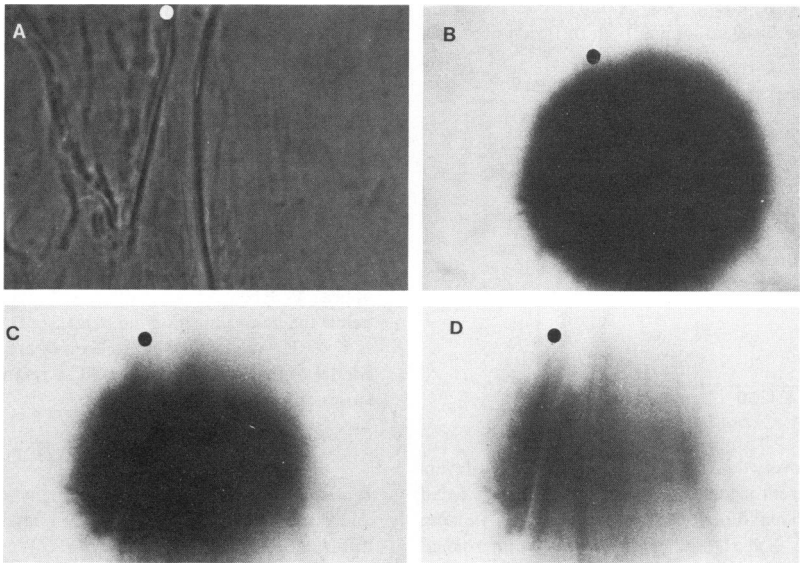

FIGURE 4 Photographs of fluorescence recovery along paired disclinations at 18°C. (*a*) phase contrast mapping of disclinations, (*b*) fluorescence at $t = 0$, (*c*) fluorescence at $t = 2$ h, (*d*) fluorescence at $t = 6$ h. Filled circles (•) marks the same location in each picture.

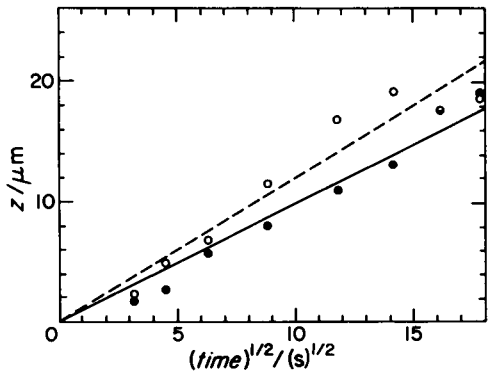

FIGURE 5 Progress of recovery as $z(C)$ along two typical disclination pairs. $z(C)$ is plotted vs. $t^{1/2}$ and fitted independently for each disclination pair.

effect is hard to observe unless the specimen is at least several microns thick and the cover glass and glass slide are extremely clean. The textured pattern appears at the L_α to $P_{\beta'}$ phase transition. It exists in all parts of the thicker specimens. A slight flow of material at the phase transition often produces large domains with the stripes oriented in the flow direction. During this flow, the paired disclinations lose their characteristic undulations (Schneider and Webb, manuscript in preparation). More frequently, the mosaic domains are so small as to be barely resolvable, so that there is an appearance of graininess that has previously been reported by others (11).

The photomicrographs in Fig. 7 show a pattern of fluorescence recovery after the upper half space of a region of large aligned domains has been photobleached; Fig. 7 *a* was photographed immediately after photobleaching and Fig. 7 *b* was photographed after 6 h of recovery. A comparison of Figs. 6 and 7 shows that there is fast recovery where the stripes in the textured pattern are aligned perpendicular to the edge of the photobleached area. This result is seen even in the absence of nearby paired disclinations. The diffusivity along the stripes in Fig. 7 seems to be comparable with that of the adjacent paired disclinations. Thus, fast diffusion is associated with large striped domains that happen to be suitably aligned as well as with paired disclinations. The variable domain alignments at the photobleached interface cause the interface to appear noticeably ragged after six hours of recovery, as noted at the end of the last section.

A BANDED DISORDER MODEL OF THE $P_{\beta'}$ PHASE

The $P_{\beta'}$ phase is characterized by regular corrugations of the bilayers. It has been proposed that the corrugations are either sawtooth (19–21, 24, 25) or undulating (2, 6, 7, 13, 23). With either structure, intermolecular disorder allowing fast diffusion may be associated with regions of high curvature that appear every half period

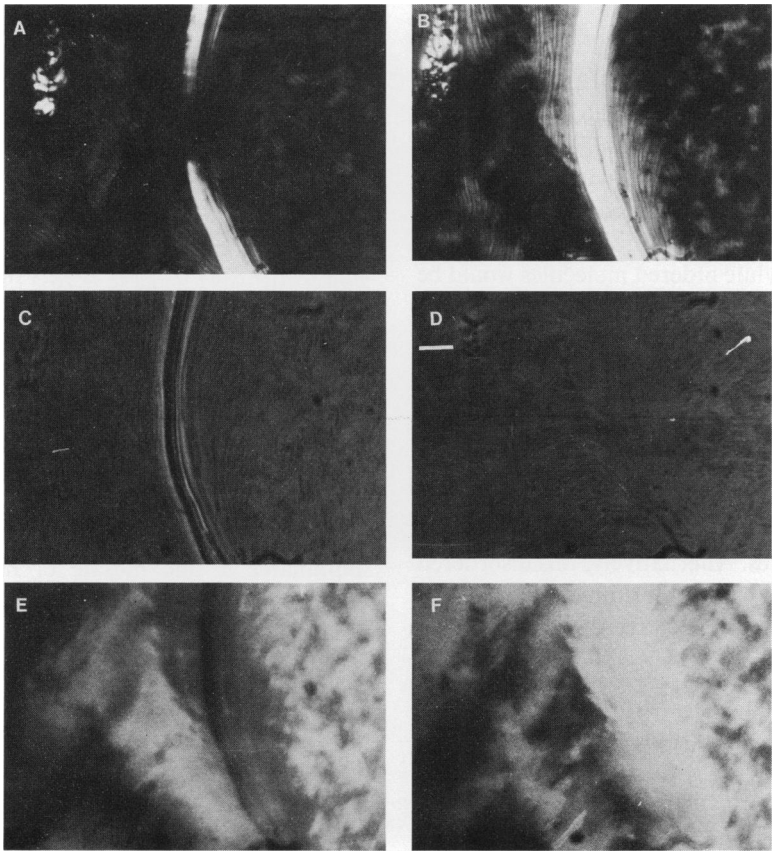

FIGURE 6 Aligned textures in the $P_{\beta'}$ phase as observed with crossed polarizers oriented (*a*) vertically and horizontally and (*b*) at 45° with respect to the edges of the frame. The stripes (and the paired disclinations) are most visible for skew orientations. Phase contrast pictures were made using a polarizer oriented (*c*) horizontally and (*d*) vertically. The stripes (and the paired disclinations) are most visible when they are perpendicular to the plane of polarization. The white bar in (*d*) is 10 μm long. Fluorescence pictures were made using plane polarized exciting light oriented (*e*) horizontally and (*f*) vertically. The striped areas (and the paired disclinations) show brightest contrast when they are parallel to the plane of polarization of the exciting light. Specimen was at 15.5°C.

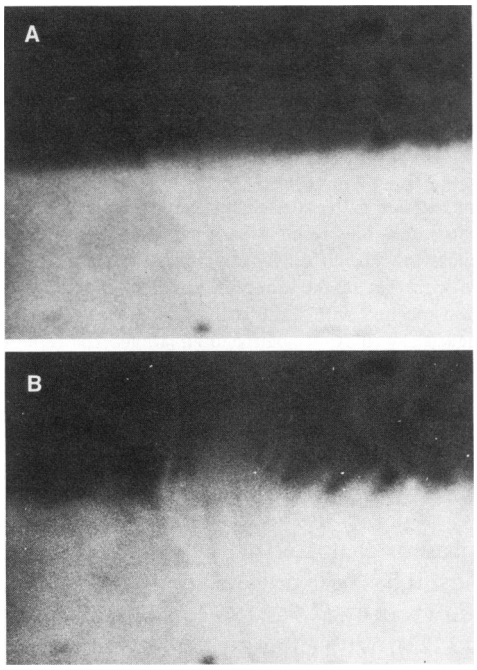

FIGURE 7 Diffusive recovery along the stripes in the textured pattern of Fig. 6. (*a*) Fluorescence distribution at $t = 0$. (*b*) Fluorescence distribution at $t = 365$ min. The recovery along the textured stripes intersecting the edge of the bleached patch is clearly visible.

(Fig. 8). The mean repeat distance, $P/2$, between the disordered bands in a bilayer is ~70 Å (2, 6, 7,13–22). We hypothesize that the bands of high intermolecular disorder are composed of a mixture of molecules with high and low intramolecular hydrocarbon chain disorder. Molecules of high-chain disorder would aggregate in the concave monolayer of the corrugations while ordered molecules would be arrayed elsewhere with their molecular axis parallel with the mean normal to the bilayer (Fig. 8). Thus we visualize the intermolecular disorder as a consequence of the inhomogeneous packing of molecules of disparate effective shape and size due to a range of hydrocarbon chain order. This is consistent with the ^{13}C magnetic resonance experiments of Griffin and co-workers (53), which detect two populations of lipid molecules in the $P_{\beta'}$ phase with different axial rotation rates. Alternatively, this disordered structure may be a natural nonequilibrium consequence of a diffusionless, shear (Martensitic) transformation from the L_α to the $P_{\beta'}$ phase as has been suggested by Chan and Webb (24).

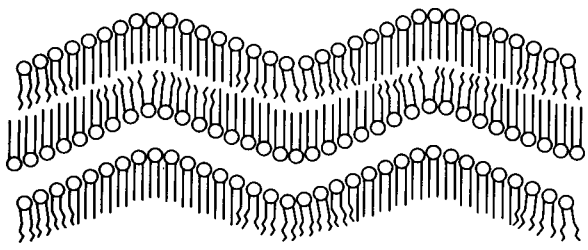

FIGURE 8 Possible model of the corrugated structure for the $P_{\beta'}$ phase showing intermolecular and intramolecular disorder situated mainly in the concave monolayer.

The submicroscopic disordered band model explains the observed diffusive behavior in the paired disclinations and striped texture regions. The optical properties of the paired disclinations indicate that the bilayers are still intact. The quasi-crystallinity of the $P_{\beta'}$ phase implies that the bilayers are highly resistant to bending but are locally stabilized in nonzero curvature. However, over microscopic distances, the intermolecularly disordered bands effectively reduce the intralayer splay elastic constant around one axis. The curvature associated with the paired disclinations aligns the corrugations parallel to the disclinations and gives rise to the observed fast diffusion along these macroscopic defects. Fast diffusion also occurs where the corrugations are adventitiously aligned over long distances by the curvature of the textured stripes. We have not established the mechanics of the formation of the visible striped texture although we have suggested that flow during the phase transformation may be responsible for this large scale anisotropy of the mosaic texture. We conjecture that the corrugations give rise to an anisotropic resistance to shear, and thus the corrugations align along the flow field.

To interpret the FPR results we consider the limiting case in which the corrugations of the $P_{\beta'}$ crystal are well aligned on a macroscopic scale maximizing the diffusion anisotropy. In this model, parallel bands, $(1 - f')P/2$ wide, of ordered material with diffusion coefficient D' are separated by $f'P/2$ wide bands of disordered material with diffusion coefficient approximately equal to D_f. If $D' \ll D_f$, the fluorescence recovery observed is due to fast diffusion along the disordered bands accompanied by a slower diffusive leakage across the ordered regions. There is virtually no diffusion along the ordered bands (36–40). The correponding times observed in an FPR experiment are the time required for a tracer molecule to diffuse along a disordered band a distance equal to the laser beam radius, $\tau_f \sim w_0^2/(4\,D_f)$ and the time required for a tracer molecule to diffuse from one disordered band to another through the ordered material, $\tau_s \sim [(1 - f')P/2]^2/4D'$.

In the limit of maximum isotropy, the laser beam illuminates a fine mosaic of many randomly oriented anisotropic domains of average radius $R \ll w_0$. If each domain is encircled by a grain boundary with a diffusion coefficient much greater than D_f, the diffusion in the grain boundary would shorten the time it takes for molecules to diffuse into the fast bands located in the center of the bleached region and the fast time observed in an FPR experiment would be $\sim R^2/4D_f$. If the grain boundary diffusion coefficient is $\sim D_f$, the fast time would be a few times τ_f. The slow time would be τ_s in both cases.

In fact, the optically observed grainy texture seen in the micrometer thick specimens indicates that the $P_{\beta'}$ crystal forms at the phase transition in domains with sizes on the order of the specimen thickness. Therefore $R \sim w_0 \sim 1\ \mu m$ and the specimens are substantially anisotropic. The frac-

tion, f, of fast diffusing molecules would be expected to be fairly constant from specimen to specimen if $R \ll w_0$ but f is expected to vary, as observed (Fig. 2 *b*), if there are only a few domains in the area of the laser beam. The measured fast diffusion coefficient, D_{pd} along the anisotropic paired disclinations (Eq. 6) agrees with the estimate of the submicroscopic diffusion coefficient, D_f, in the disordered bands (Eq. 4). We conclude $f' \sim f \sim 0.5$ and the diffusion coefficient in the disordered bands is roughly equal to D_f

$$D_{disorder} = 4 \pm 3 \times 10^{-11} \text{ cm}^2/\text{s at } 16°\text{C}. \quad (7)$$

The fact that the D_f is proportional to w_0^2 if w_0 is increased implies the grain boundary diffusion coefficient is $\sim D_f$. D, the diffusion coefficient in the slow bands, is related to D_s, the slow diffusion coefficient deduced from the FPR experiments, by $D = D_s[(1 - f)P/2]^2/w_0^2$. The limits on D are

$$D \leq 2 \times 10^{-16} \text{ cm}^2/\text{s at } 22°\text{C}$$

$$D \leq 3 \times 10^{-17} \text{ cm}^2/\text{s at } 13°\text{C}. \quad (8)$$

We assume that the dye we used partitions equally well between the ordered and disordered bands of the material. Klausner and Wolf (54) have suggested that the fluorescent diI molecule with two 18-carbon chains has a slight preference for the gel phase and that the diI molecule with two 16-carbon chains shows no preference. We do not see any difference in our experiments between these two probes, or a third probe (*N*-4-nitro-benz-2-oxa-1,3-diazole phosphatidylethanolamine) (NBD-PE). We conclude that the tracer molecule behaves exactly like a lipid molecule.

The diffusion results indicate that about half of the molecules in one corrugation period (Fig. 8) are involved in defect diffusion. Just below the phase transition, the fast component of the diffusion is ~500 times slower (Fig. 2) than diffusion in the liquid crystalline L_α phase although that it is still 5,000 times faster than the slow component of diffusion. In atomic and simple molecular crystals (38, 55, 56) and organic crystals (57, 58), the ratio of a defect diffusion coefficient to the true diffusion coefficient is $\sim 10^4$ to 10^8. This suggests that the fast diffusion in our crystals may be accounted for by intermolecular disorder in the fast bands. Although the intramolecular hydrocarbon chain disorder may be substantial (53), the intermolecular order in this region is not like that of the L_α phase since D_f remains relatively small.

McConnell and co-workers (59) have suggested rather similar banding in an equilibrium $P_{\beta'}$ phase structure where the corrugation amplitude is due to the molecular length changes associated with hydrocarbon chain disorder. This model does not yield the observed amplitude of the corrugations (7, 13, 20) but would be consistent with our observed diffusion anisotropy.

We surmise that the data of references 9–11 was dominated by fast diffusion along the disordered bands. At our suggestion Derzko and Jacobson (11) have attempted to analyze their FPR results on very thick specimens in terms of two diffusion coefficients, one due to defect diffusion and the other due to bulk diffusion. Their value of D_f (10^{-10} cm^2/s $< D_f < 10^{-8}$ cm^2/s, at 13°C) is larger than any diffusion coefficient reported for DMPC in the $P_{\beta'}$ phase while their value of D_s ($\sim 5 \times 10^{-11}$ cm^2/s at 13°C) is comparable to those of Smith and McConnell (10) and of Fahey and Webb (9) and to the value we attribute to diffusion in the disordered bands (Eq. 7).

CONCLUSION

The diffusion of a fluorescent lipid analogue in the $P_{\beta'}$ phase of DMPC is dominated by fast diffusion along bands of partially disordered material with a defect diffusion coefficient of $\sim 4 \pm 3 \times 10^{-11}$ cm^2/s at 16°C. This value is approximately that attributed to bulk diffusion in earlier work (9–11). According to our analysis, the maximum value of the diffusion coefficient in ordered material of the $P_{\beta'}$ phase of DMPC is $D \leq 2 \times 10^{-16}$ cm^2/s at 22°C and $D \leq 3 \times 10^{-17}$ cm^2/s at 13°C.

We propose that the disorder responsible for much of the fast diffusion is arranged in bands associated with the ridges and furrows of the 140 Å ripples associated with the buckling of the bilayers in the $P_{\beta'}$ phase. The curvature of the molecular planes due to paired disclinations and textured stripes align the submicroscopic bands of disordered material, and hence fast diffusion is observed along these structures.

We thank Dr. Eugene A. Nothnagel and Dr. John A. Bloom for providing essential solutions of several technical problems. We thank Daniel C. Wack for helpful discussions.

We are pleased to acknowledge support from the National Science Foundation through the Materials Science Center at Cornell University and through grants PCM 8007634, DMR 8006513 and the National Institutes of Health through CA 14454C, GM 21661 and facilities provided by 5P41 27533.

Received for publication 3 March 1983 and in final form 8 April 1983.

REFERENCES

1. Chapman, D. 1968. Recent physical studies of phospholipids and natural membranes. *In* Biological Membranes. D. Chapman, editor. Academic Press, Inc., (London) Ltd., London. 1:125–202.
2. Janiak, M. J., D. M. Small, and G. G. Shipley. 1976. Nature of the thermal pretransition of synthetic phospholipids: dimyristoyl- and dipalmitoyllecthin. *Biochemistry.* 15:4575–4580.
3. Chapman, D. 1972. Nuclear magnetic resonance spectroscopic studies of biological membranes. *Ann. NY Acad. Sci.* 195:179–206.
4. Lee, A. G. 1975. Functional properties of biological membranes: a physical-chemical approach. *Prog. Biophys. Mol. Biol.* 29:5–56.
5. Cameron, D. G., H. L. Casal, H. H. Mantsch, Y. Boulanger, and I. C. P. Smith. 1981. The thermotropic behavior of dipalmitoylphosphatidylcholine bilayers. A Fourier transform infrared study of specifically labeled lipids. *Biophys. J.* 35:1–16.
6. Tardieu, A., V. Luzzati, and F. C. Reman. 1973. Structure and

polymorphism of the hydrocarbon chains of lipids: a study of lecithin-water phases. *J. Mol. Biol.* 75:711–733.
7. Janiak, M. J., D. M. Small, and G. G. Shipley. 1979. Temperature and compositional dependence of the structure of hydrated dimyristoyl lecithin. *J. Biol. Chem.* 254:6068–6078.
8. Wu, E.-S., K. Jacobson, and D. Papahadjopoulos. 1977. Lateral diffusion in phospholipid multibilayers measured by fluorescence recovery after photobleaching. *Biochemistry.* 16:3936–3941.
9. Fahey, P. F., and W. W. Webb. 1978. Lateral diffusion in phospholipid bilayer membranes and multilamellar liquid crystals. *Biochemistry.* 17:3046–3053.
10. Smith, B. A., and H. M. McConnell. 1978. Determination of molecular motion in membranes using periodic pattern photobleaching. *Proc. Natl. Acad. Sci. USA.* 75:2759–2763.
11. Derzko, Z., and K. Jacobson. 1981. Comparative lateral diffusion of fluorescent lipid analogues in phospholipid multibilayers. *Biochemistry.* 19:6050–6057.
12. Meier, P., A. Blume, E. Ohmes, F. A. Neugebauer, and G. Kothe. 1982. Structure and dynamics of phospholipid membranes: an electron spin resonance study employing biradical probes. *Biochemistry.* 21:526–534.
13. Stamatoff, J., B. Feuer, H. J. Guggenheim, G. Tellez, and T. Yamane. 1982. Amplitude of rippling in the $P_{\beta'}$ phase of dipalmitoylphosphatidylcholine bilayers. *Biophys. J.* 38:217–226.
14. Inoko, Y., and T. Mitsui. 1978. Structural parameters of dipalmitoyl phosphatidylcholine lamellar phases and bilayer phase transitions. *J. Phys. Soc. Jap.* 44:1918–1924.
15. Inoko, Y., T. Mitsui, K. Ohki, T. Sekiya, and Y. Nozawa. 1980. X-ray and electron microscopic studies on the undulated phase in lipid/water systems. *Phys. Status Solidi.* 61:115–121.
16. Pinto da Silva, P. 1971. Freeze-fracture of dipalmitoyl lecithin vesicles. *J. Microsc. (Oxf.). 12:185–192.*
17. Ververgaert, P. H. J. T., A. J. Verkleij, P. F. Elbers, and L. L. M. van Deenen. 1973. Analysis of the crystallization process in lecithin liposomes: a freeze-etch study. *Biochim. Biophys. Acta.* 311:320–329.
18. Luna, E. J., and H. M. McConnell. 1977. The intermediate monoclinic phase of phosphatidylcholines. *Biochim. Biophys. Acta.* 466:381–392.
19. Gebhardt, C., H. Gruler, and E. Sackmann. 1977. On domain structure and local curvature in lipid bilayers and biological membranes. *Z. Naturforsh. Teil C. Biochem. Biophys. Biol. Virol.* 32:581–596.
20. Krbecek, R., C. Gebhardt, H. Gruler, and E. Sackmann. 1979. Three dimensional microscopic surface profiles of membranes reconstructed from freeze etching electron micrographs. *Biochim. Biophys. Acta.* 554:1–22.
21. Sackmann, E., D. Ruppel, and C. Gebhardt. 1980. Defect structure and texture of isolated bilayers of phospholipids and phospholipid mixtures. *In* Liquid Crystals of One- and Two-dimensional order. W. Helfrich and G. Heppke, editors. Springer-Verlag New York, Inc., New York. 309–326.
22. Copeland, B. R., and H. M. McConnell. 1980. The rippled structure in bilayer membranes of phosphatidylcholine and binary mixtures of phosphatidylcholine and cholesterol. *Biochim. Biophys. Acta.* 599:95–109.
23. Doniach, S. 1979. A thermodynamic model for the monoclinic (ripple) phase of hydrated phospholipid bilayers. *J. Chem. Phys.* 70:4587–4596.
24. Chan, W. K., and W. W. Webb. 1981. Possible martensitic transformation in hydrated phospholipid liquid crystals. *Phys. Rev. Lett.* 46:39–42.
25. Cevc, G., B. Zeks, and R. Podgornik. 1981. The undulations of hydrated phospholipid multilayers may be due to water-mediated bilayer-bilayer interactions. *Chem. Phys. Lett.* 84:209–212.
26. Fuldner, H. H. 1981. Characterization of a third phase transition in multilamellar dipalmitoyllecithin liposomes. *Biochemistry.* 20:5707–5710.
27. Ruocco, M. J., and G. G. Shipley. 1982. Characterization of the subtransition of hydrated dalpalmitoylphosphatidylcholine bilayers. *Biochim. Biophys. Acta.* 684:59–66.
28. Nagle, J. F., and D. A. Wilkinson. 1982. Dilatometric studies of the subtransition in DPPC. *Biochemistry.* 21:3817–3821.
29. Webb, W. W. 1976. Applications of fluorescence correlation spectroscopy. *Q. Rev. Biophys.* 9:49–68.
30. Saffman, P. G., and M. Delbruck. 1975. Brownian motion in biological membranes. *Proc. Natl. Acad. Sci. USA.* 72:3111–3113.
31. Halperin, B. I., and D. R. Nelson. 1978. Theory of two-dimensional melting. *Phys. Rev. Lett.* 41:121–124.
32. Birgeneau, R. J., and J. D. Litster. 1978. Bond orientational order model for smectic B liquid crystals. *J. Phys. (Paris).* 39:L399–402.
33. Devaux, P., and H. M. McConnell. 1972. Lateral diffusion in spin labeled phosphatidylcholine multilayers. *J. Am. Chem. Soc.* 94:4475–4481.
34. Trauble, H., and E. Sackmann. 1972. Studies of the crystalline-liquid crystalline phase transition of lipid model membranes. III. Structure of a steroid-lecithin system below and above the lipid phase transition. *J. Am. Chem. Soc.* 94:4499–4510.
35. Lee, A. G., N. J. M. Birdsall, and J. C. Metcalfe. 1973. Measurement of fast lateral diffusion of lipids in vesicles and in biological membranes by proton nuclear magnetic resonance. *Biochemistry.* 12:1650–1659.
36. Harrison, L. G. 1961. Influence of dislocations on diffusion kinetics in solids with particular reference to the alkali halides. *Faraday Soc. Trans.* 57:1191–1199.
37. Hart, E. W. 1957. On the role of dislocations in bulk diffusion. *Acta Met.* 5:597.
38. Fisher, J. C. 1951. Calculation of diffusion penetration curves for surface and grain boundary diffusion. *J. Appl. Phys.* 22:74–77.
39. Whipple, R. T. P. 1954. Concentration contours in grain boundary diffusion. *Phil. Mag.* 45:1225–1236.
40. LeClaire, D. D. 1963. The analysis of grain boundary diffusion measurements. *Brit. J. Appl. Phys.* 14:351–356.
41. Owicki, J. C., and H. M. McConnell. 1980. Lateral diffusion in inhomogeneous membranes. Model membranes containing cholesterol. *Biophys. J.* 30:383–398.
42. Kleman, M., C. Colliex, and M. Veyssie. 1976. Recognition of defects in water-lecithin L_α phases. *Adv. Chem. Ser.* 152:71–84.
43. Asher, S. A., and P. S. Pershan. 1979. Alignment and defect structures in oriented phosphatidylcholine multilayers. *Biophys. J.* 27:393–422.
44. Sims, P. J., A. S. Waggoner, C. H. Wang, and J. F. Hoffman. 1974. Studies on the mechanism by which cyanine dyes measure membrane potential in red blood cells and phosphatidylcholine vesicles. *Biochemistry.* 13:3315–3330.
45. Chan, W. K., and W. W. Webb. 1981. Determination of the permeation coefficient in a lyotropic smectic liquid crystal by annealing elementary edge dislocations. *Phys. Rev. Lett.* 46:603–606.
46. Chan, W. K., and W. W. Webb. 1981. Observation of elementary edge dislocations in phospholipid multilayers and of their annealing as a determination of the permeation coefficient. *J. Phys. (Paris).* 42:1007–1013.
47. de Gennes, P. G. 1974. The Physics of Liquid Crystals. Oxford University Press, London. 277–305.
48. Poo, M.-M., and R. A. Cone. 1974. Lateral diffusion of rhodopsin in the photoreceptor membrane. *Nature (Lond.).* 247:438–441.
49. Axelrod, D., D. E. Koppel, J. Schlessinger, E. Elson, and W. W. Webb. 1976. Mobility measurement by analysis of fluorescence photobleaching recovery kinetics. *Biophys. J.* 16:1055–1069.

50. Koppel, D. E., D. Axelrod, J. Schlessinger, E. L. Elson, and W. W. Webb. 1976. Dynamics of fluorescence marker concentration as a probe of mobility. *Biophys. J.* 16:1315–1329.
51. Schneider, M. B., and W. W. Webb. 1981. Measurement of submicron laser beam radii. *Appl. Opt.* 20:1382–1388.
52. Jost, W. 1952. Diffusion in Solids, Liquids, Gases. Academic Press, Inc., New York. 20.
53. Wittebort, R. J., C. F. Schmidt, R. G. Griffin. 1981. Solid-state carbon-13 nuclear magnetic resonance of the lecithin gel to liquid-crystalline phase transition. *Biochemistry.* 20:4223–4228.
54. Klausner, R. D., and D. E. Wolf. 1980. Selectivity of fluorescent lipid analogues for lipid domains. *Biochemistry.* 19:6199–6203.
55. Levine, H. S., and C. J. MacCallum. 1960. Grain boundary and lattice diffusion in polycrystalline bodies. *J. Appl. Phys.* 31:595–599.
56. Pavlov, P. V., V. A. Panteleev, and A. V. Maiorov. 1964. Diffusion of antimony along dislocations in silicon. *Sov. Phys. Solid State.* 6:305–310.
57. Sherwood, J. N., and D. J. White, 1967. Self-diffusion in naphthalene single crystals. *Phil. Mag.* 15:745–753.
58. Sherwood, J. N., and D. J. White. 1967. Self-diffusion in polycrystalline naphthalene. *Phil. Mag.* 16:975–980.
59. Falkovitz, M. S., M. Seul, H. L. Frisch, and H. M. McConnell. 1982. Theory of periodic structures in lipid bilayer membranes. *Proc. Natl. Acad. Sci. USA.* 79:3918–3921.